Solar Phys (2017) 292:157
DOI 10.1007/s11207-017-1171-7

Comparison of CME and ICME Structures Derived from Remote-Sensing and *In Situ* Observations

V. Bothmer[1] · **N. Mrotzek**[1]

Received: 26 October 2016 / Accepted: 8 September 2017 / Published online: 18 October 2017

Abstract We present results from the comparison of the near-Sun and *in situ* analysis of two Earth-directed coronal mass ejections (CMEs) with different 3D orientations and solar source region characteristics. The CME on 14 July 2000, the so-called Bastille Day storm, a well-studied event, was observed from a single-point perspective by the *Large Angle and Spectrometric Coronagraph* (LASCO) onboard the *Solar and Heliospheric Observatory* (SOHO). It caused a major geomagnetic storm with a peak Kp of 9. The CME originated from a magnetic bipolar photospheric source region with the polarity inversion line being oriented rather parallel to the heliographic equator. In contrast, the CME on 29 September 2013, which caused a geomagnetic storm with a peak Kp intensity of 8-, originated from a magnetic quadrupolar photospheric source region with the polarity inversion line between the two bipoles almost vertically oriented with respect to the heliographic equator. The results of a graduated cylindrical shell (GCS) analysis of the CMEs near the Sun are compared with the minimum variance analysis (MVA) of the magnetic field structure of the interplanetary CME (ICME) measured *in situ* near Earth's orbit. The results are in good agreement for the September 2013 CME and ICME, whereas the July 2000 ICME appears substantially inclined near Earth's orbit. The discrepancy can likely be explained taking into account kinks in the CME's near-Sun structure of the CME that expands into the interplanetary medium.

Keywords Coronal mass ejection · Space weather

Earth-affecting Solar Transients
Guest Editors: Jie Zhang, Xochitl Blanco-Cano, Nariaki Nitta, and Nandita Srivastava

✉ V. Bothmer
bothmer@astro.physik.uni-goettingen.de

N. Mrotzek
nmrotzek@astro.physik.uni-goettingen.de

[1] Institute for Astrophysics, Georg-August-University Goettingen, Goettingen, Germany

1. Introduction

Impulsive expulsions of magnetised plasma from the solar corona are called coronal mass ejections (CMEs, see *e.g.* Gosling, 1990; Webb and Howard, 2012). Fast CMEs are the drivers of major space weather effects in the heliosphere (*e.g.* Bothmer and Daglis, 2007; Gopalswamy, 2016). The strongest geomagnetic storms can be linked to the impact of interplanetary CMEs (ICMEs) on Earth's magnetosphere (*e.g.* Bothmer and Schwenn, 1995). The strength of a geomagnetic storm depends on the first order on two main characteristics of the ICME: its velocity, v, and the strength of its southward magnetic field, B_z, in geocentric solar magnetospheric (GSM) coordinates (*e.g.* Murayama, 1982; Lockwood *et al.*, 2013). CMEs were first detected in the early 1970s by coronagraphs onboard the *Orbiting Solar Observatory* (OSO) 7 and *Skylab* (Tousey, Howard, and Koomen, 1974; Gosling *et al.*, 1974). To date, we are in a unique situation because we are able to observe CMEs from multipoint perspectives with coronagraphs onboard the twin *Solar Terrestrial Relations Observatory* spacecraft (STEREO: Kaiser, 2005) and onboard the *Solar and Heliospheric Observatory* (SOHO: Domingo, Fleck, and Poland, 1995). To study the solar source regions of CMEs and their *in situ* properties at 1 AU, SOHO/*Extreme Ultraviolet Imaging Telescope* (EIT: Delaboudinière *et al.*, 1995) and *Michelson Doppler Imager* (MDI: Scherrer *et al.*, 1995), *Solar Dynamics Observatory* (SDO: Pesnell, Thompson, and Chamberlin, 2012)/*Advanced Imaging Assembly* (AIA: Lemen *et al.*, 2012) and *Helioseismic Magnetic Imager* (HMI: Schou *et al.*, 2012) data and *in situ* solar wind measurements of the *Advanced Composition Explorer* (ACE: Stone *et al.*, 1998) have been investigated.

The SOHO/*Large Angle and Spectrometric Coronagraph* (LASCO: Brueckner *et al.*, 1995) C2 and C3 coronagraphs led Cremades and Bothmer (2004) to investigate the typical three-part structure of CMEs, consisting of a bright front, a dark cavity, and a bright core containing prominence material (Fisher and Poland, 1981; Illing and Hundhausen, 1985) with respect to the structure of their low coronal and photospheric source regions. The authors found that the topology of CMEs observed in the LASCO C2 field of view (FOV) can be classified according to a basic scheme in which the fundamental parameters are the heliographic position and orientation of the source region (SR) neutral line separating the opposite magnetic polarities and the overlying magnetic loops. The three-part structure can be explained with a magnetic flux rope (FR) configuration that depends on the SR magnetic polarity orientation and the hemispheric helicity dependence (Bothmer and Schwenn, 1998), supporting the findings by Marubashi (1986). Riley *et al.* (2008) showed with magnetohydrodynamics (MHD) simulations that the FR corresponds to the dark cavity, and that the post-shock sheath material identified in *in situ* observations can be explained as piled-up ambient solar wind material ahead of the bright leading edge. In December 2008, when the two STEREO satellites were separated by about 90° in ecliptic longitude, a flux rope structure was found to match the stereoscopic CME observations, with the event being tracked all along the Sun–Earth line (Davis *et al.*, 2009; DeForest, Howard, and McComas, 2013). The graduated cylindrical shell model (GCS), describing a flux rope configuration, developed by Thernisien, Howard, and Vourlidas (2006), based on the CME scheme proposed by Cremades and Bothmer (2004), has become a widely accepted modelling method (Thernisien, 2011; Bosman *et al.*, 2012). The magnetic flux rope nature of CMEs in coronagraph observations is further supported by the studies of Vourlidas *et al.* (2013) and Vourlidas (2014). Bothmer (2003) has reported a number of uniquely associated ICMEs measured by ACE and *Wind* near 1 AU whose magnetic configuration matched the basic magnetic cloud (MC) scheme introduced by Bothmer and Schwenn (1998) and Bothmer and Rust (2013). A recent study by Marubashi *et al.* (2015) supports this view and further considers cases in which

CMEs may have been hit *in situ* at their flanks rather than near their cores. However, there are also studies where the magnetic configurations inferred *in situ* do not seem to match those derived from the associated photospheric SRs (*e.g.* Yurchyshyn *et al.*, 2001). Savani *et al.* (2015) have pointed out that modifications to the simplified Bothmer and Schwenn (1998) scheme may be applied to CME source regions with quadrupolar field configurations. This was also indicated by Bothmer and Zhukov (2007), who also mentioned that FR structures could be more complex in cases of underlying photospheric fields with curved and kinked polarity inversion lines and through interactions of CMEs with ambient coronal fields. Detailed studies connecting SR characteristics and CME remote-sensing and *in situ* ICME observations are therefore important to further clarify the underlying physical mechanisms and to enable more reliable space weather forecasts. This is the aim of this study, in which we present two case studies of near disc-centred SRs that caused Earth-directed ICMEs. The event in July 2000 is the so-called Bastille Day storm, which has been the subject of a number of studies (*e.g.* Manoharan *et al.*, 2001). The other event was observed in September 2013. Section 2 describes the remote-sensing and *in situ* observations, followed by an analysis of the data in Section 3 and a summary of the results in Section 4.

2. Observations

2.1. CME on 14 July 2000

On 14 July 2000, EIT onboard the SOHO satellite observed a strong flare released from NOAA active region (AR) 9077, located near the solar equator, close to the central meridian (N16.8 E0.21) at 10:13 UT. The flare reached an X-ray level of X5.7 and is well known as the Bastille Day event. It has been discussed in a number of articles published in *Solar Physics* (204, issue 1 – 2, 2001). The first two rows of Figure 1 show the flare and CME SR location in EIT 304 Å images at 07:19 UT and at 12:36 UT, *i.e.* before and after the flare onset and CME ejection. The EIT images have been processed with SolarSoft[1] routines. The corresponding MDI line-of-sight magnetograms at 08:00 UT are shown in the bottom row of Figure 1. After the flare, a post-eruptive arcade (PEA) was visible in EIT 304 Å along the neutral line of AR 9077, a typical coronal signature associated with CME events (Tripathi, Bothmer, and Cremades, 2004; Cremades and Bothmer, 2004).

The CME associated with this flare was visible in LASCO C2 at 10:54 UT as a full-halo CME (Bothmer and Daglis, 2007). It is only visible in a few C2 and C3 images because of solar energetic particle (SEP) impacts on the LASCO CCDs. Figures 2a and b show the GCS FR fits. The specific results are discussed in Section 3 together with the analysis of the *in situ* measurements.

The solar wind measurements from the *Wind* satellite, shown in Figure 3, reveal that the ICME arrived at L1, around 19:00 UT on 15 July, after a transit time (TT) of 33 hours, discernible through the intense solar wind magnetic field strength and out of ecliptic field rotation from south to north, as visible in the polar angle, θ_B. The ICME is preceded by a shock wave, noticeable as a jump to about 1100 km s^{-1} in the velocity measurements at 14:35 UT (Bothmer and Daglis, 2007). The ICME caused an intense geomagnetic storm with a Kp of 8, 9-, 9, and 9- during the daily fifth, sixth, seventh, and eighth three-hour intervals on 15 July and 8- during the first three hours on 16 July. A peak minimum Dst

[1] http://www.lmsal.com/solarsoft/.

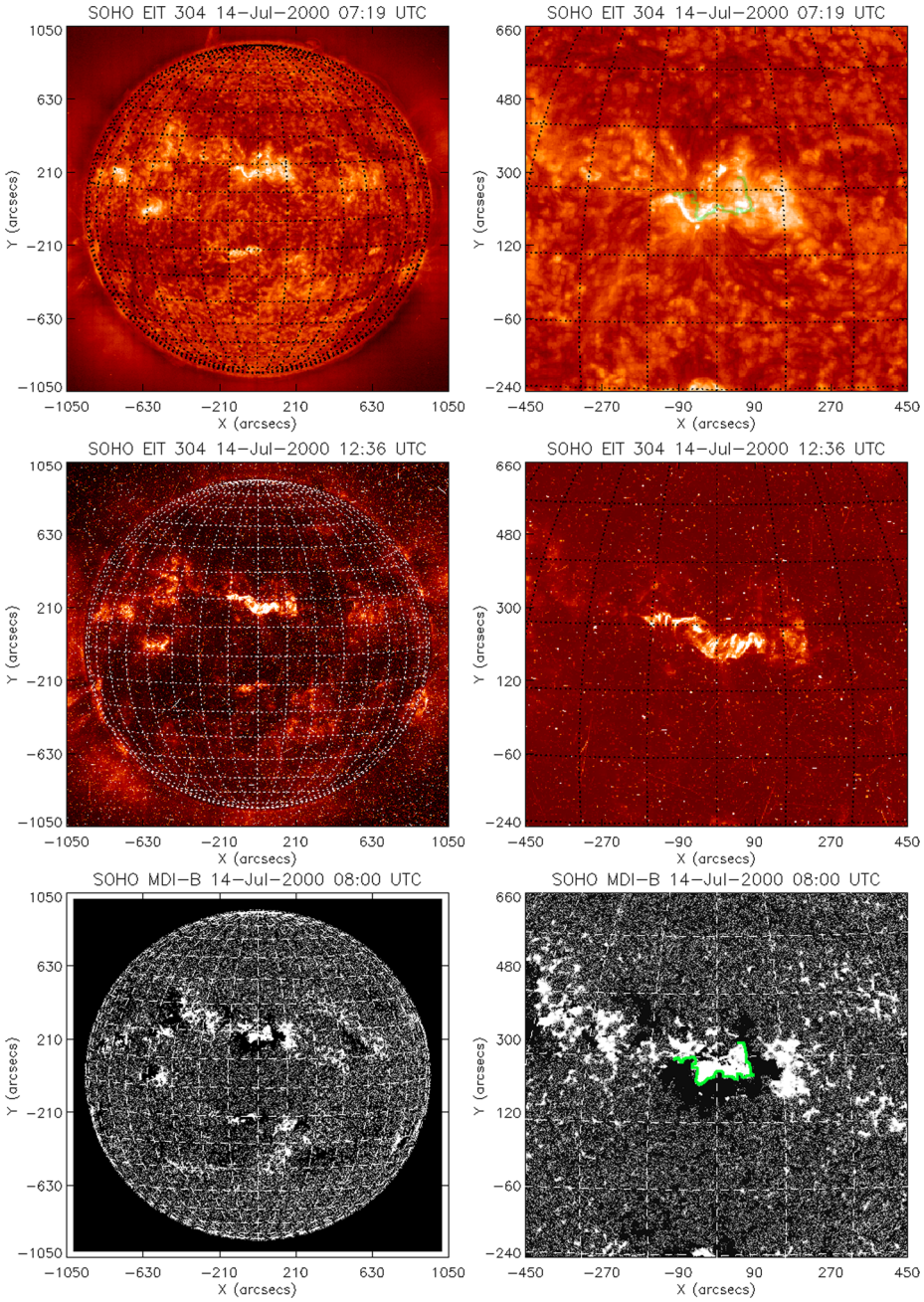

Figure 1 SR for the July 2000 CME event observed with SOHO/EIT and MDI. *Top row*: EIT 304 Å image taken at 07:19 UT. The SR is located at the central meridian and north of the heliographic equator. *Middle row*: EIT images taken at 12:36 UTC showing the typical PEAs after the CME launch. *Bottom row*: MDI line-of-sight magnetogram showing the magnetic structure of the CME photospheric SR. *Black* denotes the magnetic polarity directed towards the Sun, *white* denotes opposite-directed fields. The polarity inversion line is shown in *green* in the zoom in the *right-hand bottom* panel.

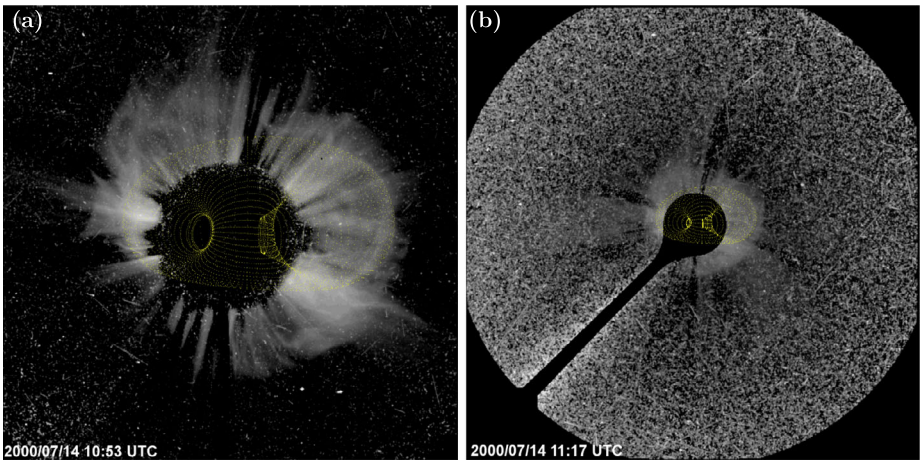

Figure 2 GCS modelling results of the Bastille Day event seen by (**a**) SOHO/LASCO C2 at 10:53 UTC and (**b**) C3 at 11:17 UTC. The *yellow grid* shows the FR fitted with the GCS model. The noise in image in panel (**b**) is a result of SEPs oversaturating pixels of the CCD.

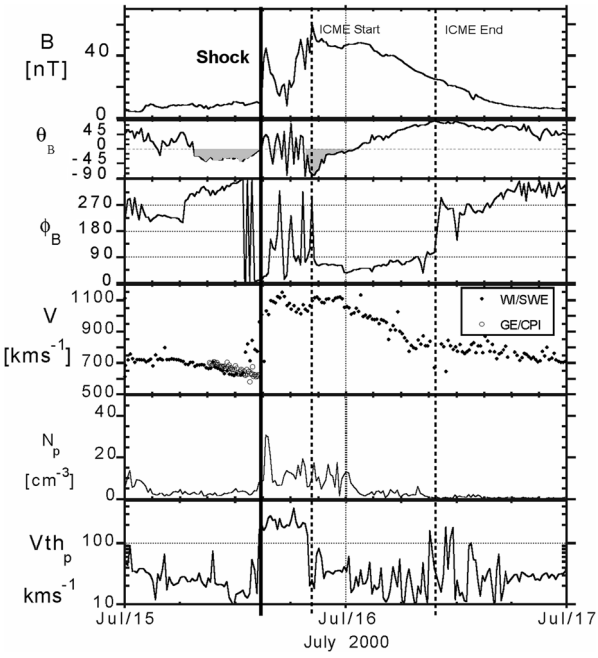

Figure 3 Solar wind parameters measured by the *Wind* and *Geotail* satellites from 15 to 17 July 2000. From top to bottom: total magnetic field magnitude, B, polar angle, θ_B, azimuthal angle, ϕ_B, proton velocity, v, proton number density, N_p, and thermal velocity of protons, vth_p. The shock arrival is marked by a solid line, while the ICME start and end times are labelled with *dashed lines*. Adapted from Bothmer and Daglis (2007). Courtesy: Lepping *et al.* (2001).

value of −301 nT was reported by the Kyoto World Data Center for Geomagnetism.[2] The analysis of the *in situ* magnetic field structure of the ICME is discussed in Section 3 together with the GCS results.

[2] http://wdc.kugi.kyoto-u.ac.jp/.

2.2. CME on 29 September 2013

A large filament disappearance was observed around 20:00 UT on 29 September 2013, as shown in the SDO/AIA images in the top row of Figure 4. It should be noted that in association with this event, a C1.2 class X-ray flare was detected at 21:43 UT at N10 W33. The location of the elongated filament in the top right image of Figure 4 was N40 W20 to N5 W40, *i.e.* it was oriented almost normal to the solar equator, with a reverse S-shaped structure typical for the northern hemispheric events (Canfield, Hudson, and McKenzie, 1999).

The SDO/HMI observations shown in the bottom row of Figure 4 reveal that the filament was located between two bipolar regions above which a post-eruptive arcade formed after the CME liftoff (Figure 4, middle row). A detailed characterisation of the filament, the photospheric SR, and the eruption details can be found in Palacios *et al.* (2015). The associated CME was first observed in the FOV of the *Sun Earth Connection Coronal and Heliospheric Investigation* (SECCHI: Howard *et al.*, 2008) COR1 A instrument, onboard STEREO, on 29 September at 21:45 UT. In the COR1 A, COR2 A, C2, and C3 images, the CME appears as a partial halo, while a full halo was seen in COR1 B and COR2 B. The multipoint observations of the evolving CME are shown in Figure 5 together with the GCS modelled FR grid that is applied to all three viewing perspectives and the positions of the three satellites. The specific GCS results for the July 2000 event are discussed in Section 3 together with the analysis of the *in situ* ICME magnetic field data. It is obvious from Figure 5 that the filament material appears in remarkable detail in the different coronagraph images, while the bright shock material ahead of the CME is only clearly visible in COR2 A and B. Shocks in white-light images have previously been identified and interpreted by Sheeley *et al.* (1999), Vourlidas and Ontiveros (2009) and analysed by Volpes and Bothmer (2015). A good overview on CME and shock research has been provided by Gopalswamy (2016). According to the *in situ* solar wind data of ACE shown in Figure 6, the ICME shock arrived at 02:00 UT on 2 October 2013, as identified from simultaneous jumps in the hourly averages of the magnetic field magnitude, B, from 5 nT to 20 nT, with a subsequent peak value of 33 nT, and the solar wind velocity, v, increasing from below 400 km s^{-1} to around 600 km s^{-1}. Gaps in the data are due to missing availability of ACE science level 2 data. The arrival time of the ICME leading edge is identified from the drop in the solar wind density and temperature measurements around 00:00 UT on 3 October, which implies a TT of the ICME of about 76 hours. In this case, a geomagnetic storm with a peak Kp of 8- in the three-hour interval from 3:00 to 6:00 UT on 2 October was triggered. The peak minimum Dst was only −60 nT as reported in the provisional Dst data provided by the Kyoto World Data Center for Geomagnetism. The results of the analysis of the ICME magnetic field structure are discussed together with the GCS results in Section 3.

3. Analysis and Results

3.1. Near-Sun GCS Modelling of CMEs

To model the CME near-Sun global structure, the GCS method, as described in Thernisien, Howard, and Vourlidas (2006), was applied to both events using time series of processed images from the STEREO/SECCHI COR1 A and B, COR2 A and B, and SOHO/LASCO C2 and C3 instruments. Only LASCO C2 and C3 data exist for the first event, but because of the overall set of observations, this fact was not considered to be critical to compare the two selected events. For a detailed discussion of the uncertainties of the GCS parameters, we

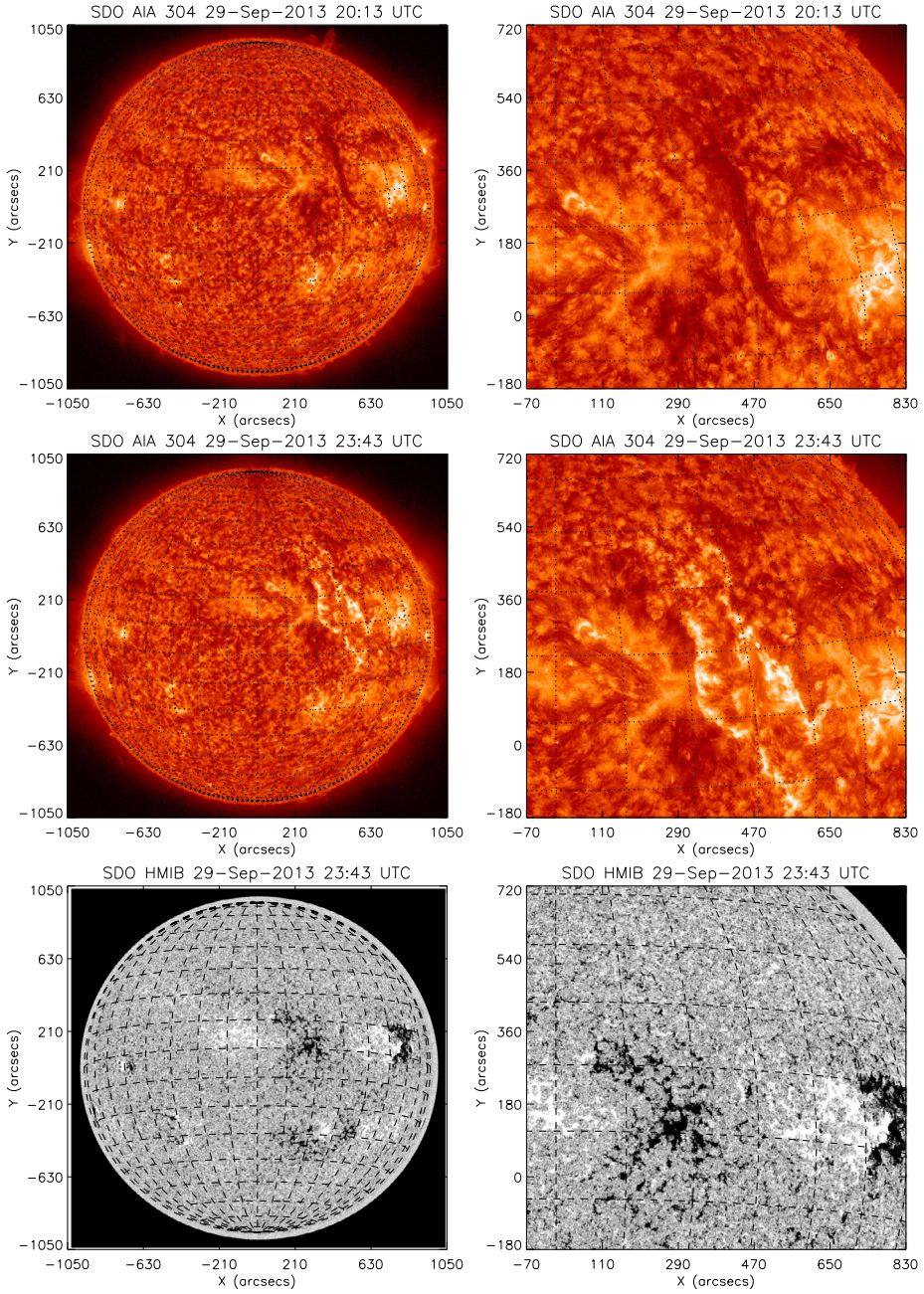

Figure 4 SR for the 29 September 2013 CME event observed with SDO/AIA and HMI. *Top row*: SDO/AIA 304 Å images taken at 20:13 and 23:43 UTC showing a large filament. *Middle row*: The PEA after the disappearance of the filament. Zoomed images are shown in the *right column*. *Bottom row*: SDO/HMI magnetograms taken at 23:43 UT. The filament was located between two large bipolar magnetic regions.

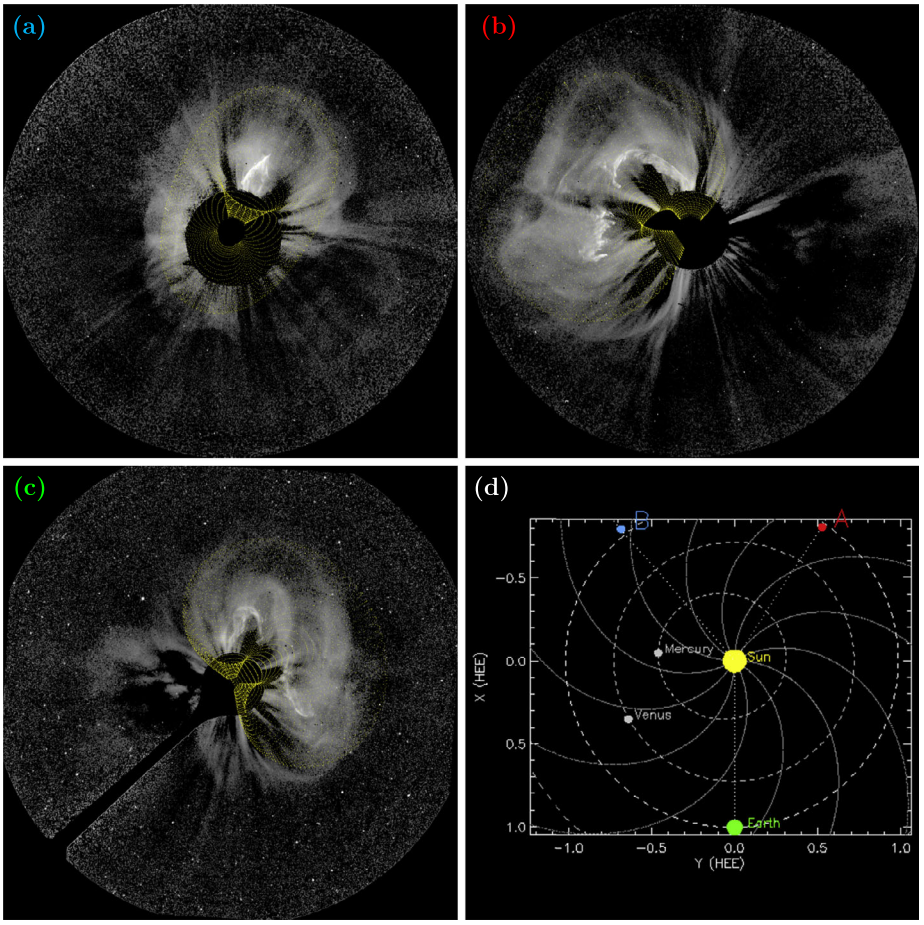

Figure 5 Event on 29 September 2013 observed by the coronagraphs. (**a**) and (**b**): STEREO/COR 2A and B images at 23:39 UT. (**c**): SOHO/LASCO C3 at 01:39 UT 30 September 2013 image. The modelled GCS flux rope is represented by the *yellow grid*. (**d**): The positions of the satellites are shown with the STEREO Orbit Tool (http://stereo-ssc.nascom.nasa.gov/where.shtml).

refer to the statistical results of Thernisien, Vourlidas, and Howard (2009). The error of the GCS tilt angle, derived from the fitting procedures, is found to be of the order of 22°. In the case of the July 2000 CME, for which only single-point SOHO observations were available, the height, h, the half-angle, α, and the aspect ratio, κ, cannot be fitted fully independently of each other. The full GCS parameters cannot be derived, but the determined orientation is expected to be close to the true orientation because of the disc-centred SR orientation and the face-on view of the CME, which propagated towards the Earth's orbit. Moreover, the identification of bright CME features in the west and east allows a good separation of shock material and the CME body (Andrews, 2001). Because of the acceleration phase of CMEs over the first solar radii, as explained by Lorentz forces (Michalek *et al.*, 2015; Sachdeva *et al.*, 2015), the CME velocity cannot be considered to be constant. Therefore the near-Sun CME velocity was determined through height time profiles of the GCS fits near the outer edge of the COR2 FOV for a distance of 12 $R_{\odot}$, which makes the initial velocities

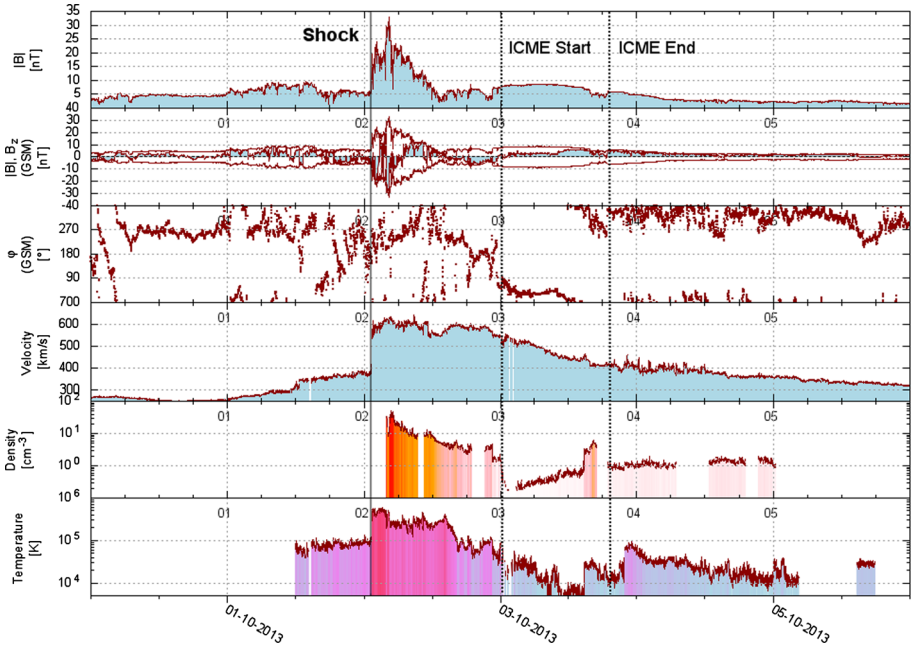

Figure 6 ACE solar wind measurements from 30 September to 6 October 2013. During the event, there were data gaps in the ACE science data in the density and temperature measurements. The parameters from top to bottom are the total magnetic field strength, $|B|$, the total magnetic field strength, $|B|$, with the B_z-component (*light blue*), the field azimuthal angle, ϕ_B, the proton velocity v, the proton density, N_p, and the temperature, T. The interplanetary shock is denoted by a *solid line*. The ICME start and end times are marked with *dashed lines*.

Table 1 GCS modelling parameters for the July 2000 and September 2013 CME events: FR apex position projected on the solar disc (coordinates are in the Carrington (Carr.) and in the heliospheric Earth equatorial coordinate system (HEEQ)), tilt angle, γ, aspect ratio, κ, and half-angle, α (Thernisien, Vourlidas, and Howard, 2009), and CME velocity, $v_{\rm ini}$, determined for a solar distance of 12 $R_\odot$ based on subsequent GCS fits under assumption of self-similar expansion. The *in situ* ICME speeds, $v_{\rm L1}$, are listed for comparison.

Event	Long. [°] (Carr.)	Long. [°] (HEEQ)	Lat. [°]	γ [°]	κ [%]	α [°]	$v_{\rm ini}$ [km s^{-1}]	$v_{\rm L1}$
2000/07/14	316	7	10	−3	0.47	70	1713^{+87}_{-122}	1100
2013/09/29	8	30	26	−68	0.59	61	1398 ± 50	550

of CMEs more comparable. The derived GCS parameters and determined velocities are summarised in Table 1 together with the *in situ* velocities and transit times for comparison. The tilt angle of the CME based on the GCS modelling was found to be $\gamma = -3°$, *i.e.* almost horizontal with respect to the solar equator. The speed decrease from 1713 km s^{-1} near the Sun to 1100 km s^{-1} at L1 is in agreement with the assumption that fast CMEs are decelerated by drag effects through interaction with the ambient solar wind (Vršnak *et al.*, 2010). The results of the GCS modelling for the 29 September 2013 CME based on multipoint observations from STEREO A and B and SOHO yielded a tilt angle of $\gamma = 68°$, in agreement with the orientation of the polarity inversion line, PEA, and filament, all being

oriented almost perpendicular to the solar equator. In this case, the kinked filament structure was also clearly visible in the coronagraph images, so that modelling in such cases likely requires more complexity. This CME has also been modelled by Wood *et al.* (2016), who obtained a similar result for the flux rope inclination. For the location of the SR on the solar disc we assume that the centre of the EUV post-eruptive arcade is a good approximation. In the July event, the SR was located at N13 E01 and in September 2013 at N08 W28. The calculated position of the FR apex with GCS was N10 W07 in July 2000 and N26 W30 in September 2013. The corresponding X-flare locations were N17 E00 in the 2000 and N10 W33 in the 2013 event. The results are in good agreement, considering that CMEs have been observed to be deflected and flares do not need to occur near the SR centre.

3.2. MVA Analysis of the *In Situ* ICME Magnetic Field Structures and Comparison with GCS Results

A commonly used method to infer the orientation of the ICME FR is the minimum variance analysis (MVA) as described in Bothmer and Schwenn (1998). The analysis was carried out for the *in situ* magnetic field data from ACE for the ICME period 15 July 19:00 UT until 16 July 9:00 UT labelled in Figure 3. It should be noted that the data shown in Figure 3 are from the *Wind* satellite, for which the plasma data have been corrected for contamination by solar energetic particles as described in Lepping *et al.* (2001). The MVA routines were standardised for the ACE dataset because of forecast tools established for the Advanced Forecast For Ensuring Communications Through Space (AFFECTS) space weather project.[3] The MVA of hourly averaged magnetic field data yielded the angles $\phi = 69°$ and $\theta = 46°$ for the direction of medium variance in the GSE system, *i.e.* the ICME axis was found to be inclined along the direction from north-east to south-west, as shown in the bottom right diagram of Figure 7. The ratio of the eigenvalues of medium to minimum variance was 2.6, thus fulfilling the required conditions for reliable MVA results.

Based on the rotation of the magnetic field vector, the magnetic cloud type of the ICME was south-east-north (SEN), *i.e.* of left-handed magnetic helicity according to the scheme introduced by Bothmer and Schwenn (1998). Compared with the polarities of the SR as inferred from the SOHO/MDI magnetogram shown in Figure 1, this is in agreement with what is expected according to the basic scheme for SR–FR–ICME relationships of northern solar hemispheric origin as proposed by Bothmer and Schwenn (1998) and Bothmer and Rust (2013). In the same way as for the July 2000 event, we applied the MVA method to ACE data for the ICME time period indicated in Figure 6. The MVA of the hourly averaged magnetic field data in this case yielded $\phi = 125°$ and $\theta = 56°$ for the direction of medium variance in the GSE system, *i.e.* the ICME axis was found to be inclined from south-west to north-east, as shown in the bottom right diagram of Figure 8. The ratio of the eigenvalues of medium to minimum variance was 13. According to the Bothmer and Schwenn scheme, in this case, the magnetic field type is east-north-west (ENW), *i.e.* of left-handed magnetic helicity, again as expected for a northern hemispheric origin of an ICME and in agreement with the photospheric magnetic polarities of the SR, as shown in the SDO/HMI magnetogram in Figure 4.

In the next step, we compare the results from the ICME MVA analysis with the results derived from the near-Sun CME GCS analysis. Since the GCS parameters are given in heliocentric Earth equatorial (HEEQ) coordinates, we transformed them into the GSE system to allow a unique comparison of the results. The effect of the inclined solar rotation axis with

[3] http://www.affects-fp7.eu.

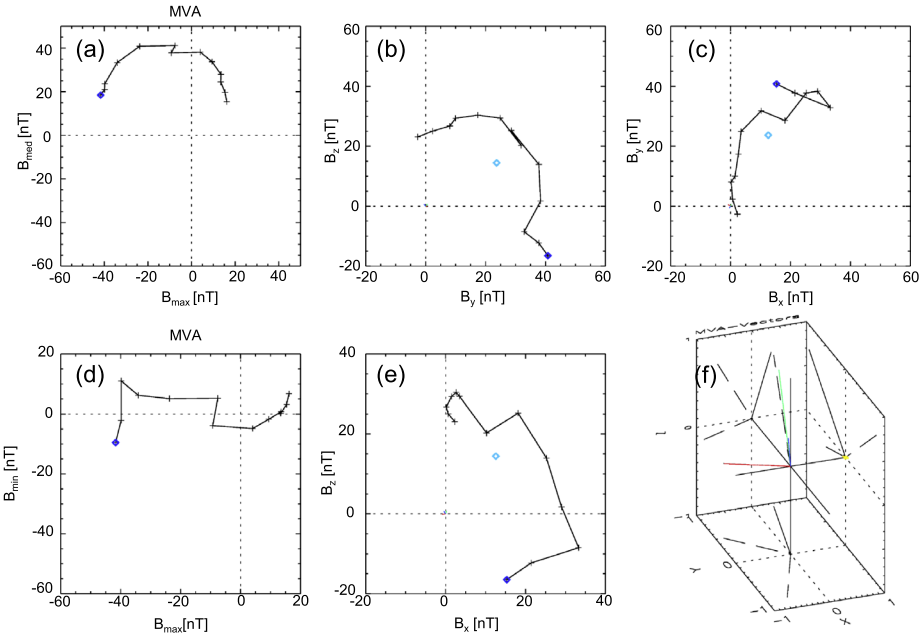

Figure 7 Results of the MVA for the ICME encountered by ACE from 15 July 2000 at 19:00 UT to 16 July 2000 9:00 UT, after a disc-centred CME liftoff on 14 July 2000. (**a**): The magnetic field rotation in the plane of maximum and medium variance. (**d**): The magnetic field variation in the plane of minimum and maximum variance. (**b**), (**c**), and (**e**): The variations in geocentric solar ecliptic (GSE) coordinates, with the blue diamond representing the average value of all data points. The units of the field strength are in nT. (**f**): The directions of the minimum (*red*) and maximum orientations in the GSE system. The FR axis, *i.e.* the direction of medium variance, is represented by the *green line*. The *yellow dot* represents the direction to the Sun.

Table 2 GCS and MVA results for the CME and ICME events. From left to right, the parameters are the GCS tilt angle, the GCS tilt angle transformed into the GSE coordinate system, the aspect ratio and half-angle, the MVA axis tilt angle, and the longitudinal direction in GSE coordinates.

Event	GCS				MVA	
	γ [°]	γ' [°]	κ [%]	α [°]	ϕ [°]	θ [°]
14 Jul. 2000	−3	1	0.47	70	69	46
29 Sep. 2013	−68	61	0.59	61	125	56

respect to the ecliptic plane is small, as expected, and is most noticeable for the September 2013 event. All values are listed in Table 2.

In the case of the September–October 2013 event, the inclination of the ICME FR axis, being $\theta = 56°$ with respect to the ecliptic plane, is in agreement with the inclination derived from the near-Sun GCS modelling. The tilt of the fitted GCS FR transformed to the GSE system is $\gamma = 61°$ with respect to the ecliptic plane. In contrast, in the July 2000 event, the inclination of the ICME FR axis, which was found to be $\theta = 46°$ with respect to the ecliptic plane in the GSE system, strongly deviates from the GCS modelling result, yielding a horizontal orientation of the near-Sun CME FR with $\gamma = 1°$. The discrepancy in this case may be explained by taking into account the kinked structure of the PEA and PIL identified

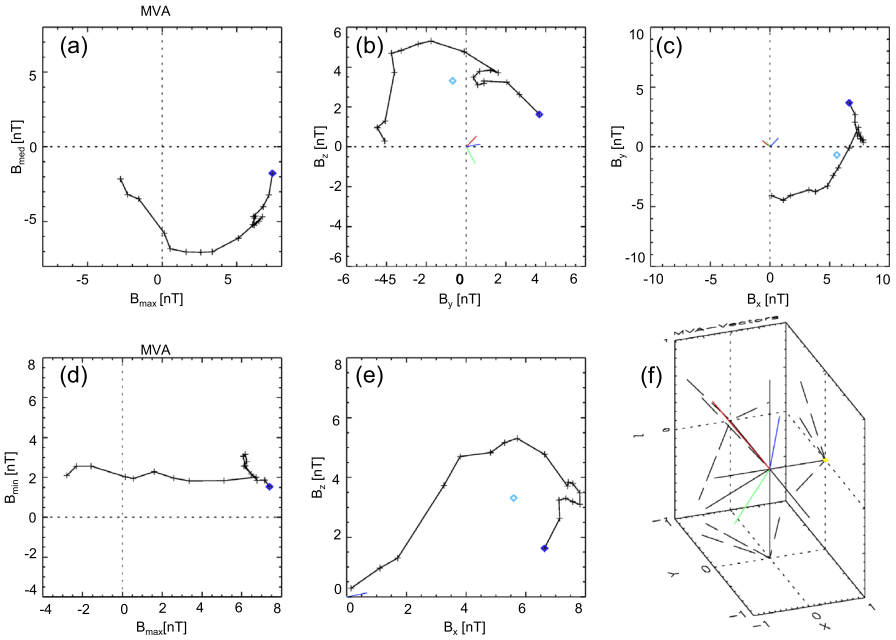

Figure 8 Results of the MVA for the ICME encountered by ACE from 3 October 2013 at 0:00 UT to 19:00 UT. (**a**): The magnetic field rotation in the plane of maximum and medium variance. (**d**): The magnetic field variation in the plane of minimum and maximum variance. (**b**), (**c**), and (**e**): The variations in geocentric solar ecliptic (GSE) coordinates, with the blue diamond representing the average value of all data points. The units of the field strength are in nT. (**f**): The directions of the minimum (*red*) and maximum orientations in the GSE system. The FR axis, *i.e.* the direction of medium variance, is represented by the *green line*. The *yellow dot* represents the direction to the Sun.

in Figure 1 assuming that this part of the overlying FR CME would have become the ICME part observed by ACE and *Wind* near Earth' s orbit.

4. Summary

We have studied two unique CME and ICME events observed in July 2000, the well-studied Bastille Day event, and in September–October 2013, for which multipoint remote-sensing observations from SOHO and STEREO were available. The solar source regions were identified in SOHO/EIT and SDO/AIA EUV observations, and the magnetic characteristics were inferred from SOHO/MDI and SDO/HMI magnetograms. The STEREO/SECCHI COR2 A and B and SOHO/LASCO C2 and C3 data were modelled with the GCS method. The *in situ* magnetic field data from the ACE satellite were analysed with the MVA method to infer the ICME magnetic field properties. We derive the following conclusions from the comparison of the *in situ* magnetic field structure with the white-light low coronal and photospheric characteristics:

- The July 2000 ICME was uniquely associated with a CME with an underlying bipolar photospheric magnetic region, whereas the CME in September 2013 was associated with an underlying quadrupolar photospheric source region.

- The ICME magnetic field structures agree with the Bothmer and Schwenn (1998) scheme when the quadrupolar magnetic field structure is taken into account for the September event. The results support the suggestion by Savani *et al.* (2015) that the basic Bothmer and Schwenn scheme has to be extended for such cases to predict the magnetic field configuration of ICMEs for such cases.
- The orientation of the ICME obtained with the MVA method applied to the *in situ* solar wind data agrees well with the orientation calculated from GCS modelling of the white-light CME observations for the September–October 2013 event.
- In contrast, in case of the July 2000 event, the derived ICME orientation differs substantially from the near-Sun CME orientation found from GCS modelling.
- In the July 2000 event, the earthward-facing portion of the photospheric source region showed a kink with a consistent inclination compared to the ICME orientation observed at 1 AU. This finding indicates that kinks in the source regions seem to be reflected in the expanded overlying FR structure that propagates into the heliosphere as a CME.
- Kinked CMEs may better be modelled through fitting different parts of the CME individually with the GCS method, which would facilitate more appropriate space weather forecasts.

The further analysis of a larger set of CME events based on mulitpoint remote-sensing observations in comparison with *in situ* measurements of ICMEs can help clarify the importance in deriving the magnetic structure of the earthward-expanding portion of the CMEs for enhancing the reliability of space weather forecasts. The results furthermore provide important aspects for more detailed studies of CMEs and ICMEs and their solar source regions with the upcoming *Parker Solar Probe* (formerly *Solar Probe Plus*), *Solar Orbiter*, and *Proba3* missions and coronagraphs that are currently being developed for future operations, such as the *Solar Coronagraph for Operations* (SCOPE: Middleton *et al.*, 2016).

Acknowledgements We thank the referee for the helpful comments that helped to improve the quality of the manuscript. This work is funded by the European Union in the FP7-Project HELCATS (Heliospheric Cataloguing, Analysis and Techniques Service). Volker Bothmer acknowledges support of the CGAUSS (Coronagraphic German And US Solar Probe Plus Survey) project for WISPR by the German Space Agency DLR under grant 50 OL 1601. The authors would like to thank Malte Venzmer and Johannes Hinrichs for providing support in solar wind data analysis. The authors acknowledge the efforts of the STEREO, SDO, and SOHO science center at GSFC, and the efforts of the STEREO/SECCHI, SDO/AIA and HMI, SOHO/LASCO, SOHO/EIT, and ACE consortia. All images were processed with SolarSoft routines.

Disclosure of Potential Conflicts of Interest The authors declare that they have no conflicts of interest.

References

Andrews, M.D.: 2001, LASCO and EIT observations of the Bastille day 2000 solar storm. *Solar Phys.* **204**(1), 179. DOI. ADS.

Bosman, E., Bothmer, V., Nisticò, G., Vourlidas, A., Howard, R.A., Davies, J.A.: 2012, Three-dimensional properties of coronal mass ejections from stereo/secchi observations. *Solar Phys.* **281**(1), 167. DOI. ADS.

Bothmer, V.: 2003, Sources of magnetic helicity over the solar cycle. In: Wilson, A. (ed.) *Solar Variability as an Input to the Earth's Environment*, *ESA* **SP-535**, 419. ADS.

Bothmer, V., Daglis, I.A.: 2007, *Space Weather – Physics and Effects*, Springer, Berlin. DOI. ADS.

Bothmer, V., Rust, D.M.: 2013, *The Field Configuration of Magnetic Clouds and the Solar Cycle*, AGU, Washington, 139. 9781118664377. DOI.

Bothmer, V., Schwenn, R.: 1995, The interplanetary and solar causes of major geomagnetic storms. *J. Geomagn. Geoelectr.* **47**(11), 1127. DOI.

Bothmer, V., Schwenn, R.: 1998, The structure and origin of magnetic clouds in the solar wind. *Ann. Geophys.* **16**, 1. DOI. ADS.

Bothmer, V., Zhukov, A.: 2007, The Sun as the prime source of space weather. In: Bothmer, V., Daglis, I.A. (eds.) *Space Weather – Physics and Effects*, Springer, Berlin, 31. DOI. ADS.

Brueckner, G.E., Howard, R.A., Koomen, M.J., Korendyke, C.M., Michels, D.J., Moses, J.D., Socker, D.G., Dere, K.P., Lamy, P.L., Llebaria, A., Bout, M.V., Schwenn, R., Simnett, G.M., Bedford, D.K., Eyles, C.J.: 1995, The Large Angle Spectroscopic Coronagraph (LASCO). *Solar Phys.* **162**, 357. DOI. ADS.

Canfield, R.C., Hudson, H.S., McKenzie, D.E.: 1999, Sigmoidal morphology and eruptive solar activity. *Geophys. Res. Lett.* **26**(6), 627. DOI.

Cremades, H., Bothmer, V.: 2004, On the three-dimensional configuration of coronal mass ejections. *Astron. Astrophys.* **422**, 307. DOI. ADS.

Davis, C.J., Davies, J.A., Lockwood, M., Rouillard, A.P., Eyles, C.J., Harrison, R.A.: 2009, Stereoscopic imaging of an Earth-impacting solar coronal mass ejection: A major milestone for the STEREO mission. *Geophys. Res. Lett.* **36**, L08102. DOI. ADS.

DeForest, C.E., Howard, T.A., McComas, D.J.: 2013, Tracking coronal features from the low corona to Earth: A quantitative analysis of the 2008 December 12 coronal mass ejection. *Astrophys. J.* **769**, 43. DOI. ADS.

Delaboudinière, J.-P., Artzner, G.E., Brunaud, J., Gabriel, A.H., Hochedez, J.F., Millier, F., Song, X.Y., Au, B., Dere, K.P., Howard, R.A., Kreplin, R., Michels, D.J., Moses, J.D., Defise, J.M., Jamar, C., Rochus, P., Chauvineau, J.P., Marioge, J.P., Catura, R.C., Lemen, J.R., Shing, L., Stern, R.A., Gurman, J.B., Neupert, W.M., Maucherat, A., Clette, F., Cugnon, P., van Dessel, E.L.: 1995, EIT: Extreme-ultraviolet imaging telescope for the SOHO mission. *Solar Phys.* **162**, 291. DOI. ADS.

Domingo, V., Fleck, B., Poland, A.I.: 1995, SOHO: The solar and heliospheric observatory. *Space Sci. Rev.* **72**, 81. DOI. ADS.

Fisher, R.R., Poland, A.I.: 1981, Coronal activity below 2 solar radii – 1980 February 15 – 17. *Astrophys. J.* **246**, 1004. DOI. ADS.

Gopalswamy, N.: 2016, History and development of coronal mass ejections as a key player in solar terrestrial relationship. *Geosci. Lett.* **3**, 8. DOI. ADS.

Gosling, J.T.: 1990, Coronal mass ejections and magnetic flux ropes in interplanetary space. In: *Physics of Magnetic Flux Ropes*, *Geophys. Monograph Ser.* **58**, AGU, Washington, 343. DOI. ADS.

Gosling, J.T., Hildner, E., MacQueen, R.M., Munro, R.H., Poland, A.I., Ross, C.L.: 1974, Mass ejections from the Sun – a view from SKYLAB. *J. Geophys. Res.* **79**, 4581. DOI. ADS.

Howard, R.A., Moses, J.D., Vourlidas, A., Newmark, J.S., Socker, D.G., Plunkett, S.P., Korendyke, C.M., Cook, J.W., Hurley, A., Davila, J.M., Thompson, W.T., St Cyr, O.C., Mentzell, E., Mehalick, K., Lemen, J.R., Wuelser, J.P., Duncan, D.W., Tarbell, T.D., Wolfson, C.J., Moore, A., Harrison, R.A., Waltham, N.R., Lang, J., Davis, C.J., Eyles, C.J., Mapson-Menard, H., Simnett, G.M., Halain, J.P., Defise, J.M., Mazy, E., Rochus, P., Mercier, R., Ravet, M.F., Delmotte, F., Auchere, F., Delaboudiniere, J.P., Bothmer, V., Deutsch, W., Wang, D., Rich, N., Cooper, S., Stephens, V., Maahs, G., Baugh, R., McMullin, D., Carter, T.: 2008, Sun Earth connection coronal and heliospheric investigation (SECCHI). *Space Sci. Rev.* **136**, 67. DOI. ADS.

Illing, R.M.E., Hundhausen, A.J.: 1985, Observation of a coronal transient from 1.2 to 6 solar radii. *J. Geophys. Res.* **90**, 275. DOI. ADS.

Kaiser, M.L.: 2005, The STEREO mission: An overview. *Adv. Space Res.* **36**, 1483. DOI. ADS.

Lemen, J.R., Title, A.M., Akin, D.J., Boerner, P.F., Chou, C., Drake, J.F., Duncan, D.W., Edwards, C.G., Friedlaender, F.M., Heyman, G.F., Hurlburt, N.E., Katz, N.L., Kushner, G.D., Levay, M., Lindgren, R.W., Mathur, D.P., McFeaters, E.L., Mitchell, S., Rehse, R.A., Schrijver, C.J., Springer, L.A., Stern, R.A., Tarbell, T.D., Wuelser, J.-P., Wolfson, C.J., Yanari, C., Bookbinder, J.A., Cheimets, P.N., Caldwell, D., Deluca, E.E., Gates, R., Golub, L., Park, S., Podgorski, W.A., Bush, R.I., Scherrer, P.H., Gummin, M.A., Smith, P., Auker, G., Jerram, P., Pool, P., Soufli, R., Windt, D.L., Beardsley, S., Clapp, M., Lang, J., Waltham, N.: 2012, The atmospheric imaging assembly (AIA) on the solar dynamics observatory (SDO). *Solar Phys.* **275**, 17. DOI. ADS.

Lepping, R.P., Berdichevsky, D.B., Burlaga, L.F., Lazarus, A.J., Kasper, J., Desch, M.D., Wu, C.-C., Reames, D.V., Singer, H.J., Smith, C.W., Ackerson, K.L.: 2001, The Bastille day magnetic clouds and upstream shocks: Near-earth interplanetary observations. *Solar Phys.* **204**(1), 285. DOI. ADS.

Lockwood, M., Barnard, L., Nevanlinna, H., Owens, M.J., Harrison, R.G., Rouillard, A.P., Davis, C.J.: 2013, Reconstruction of geomagnetic activity and near-Earth interplanetary conditions over the past 167 yr, part 1: A new geomagnetic data composite. *Ann. Geophys.* **31**, 1957. DOI. ADS.

Manoharan, P.K., Tokumaru, M., Pick, M., Subramanian, P., Ipavich, F.M., Schenk, K., Kaiser, M.L., Lepping, R.P., Vourlidas, A.: 2001, Coronal mass ejection of 2000 July 14 flare event: Imaging from near-Sun to Earth environment. *Astrophys. J.* **559**, 1180. DOI. ADS.

Marubashi, K.: 1986, Structure of the interplanetary magnetic clouds and their solar origins. *Adv. Space Res.* **6**, 335. DOI. ADS.

Marubashi, K., Akiyama, S., Yashiro, S., Gopalswamy, N., Cho, K.-S., Park, Y.-D.: 2015, Geometrical relationship between interplanetary flux ropes and their solar sources. *Solar Phys.* **290**, 1371. DOI. ADS.

Michalek, G., Gopalswamy, N., Yashiro, S., Bronarska, K.: 2015, Dynamics of CMEs in the LASCO field of view. *Solar Phys.* **290**, 903. DOI. ADS.

Middleton, K.F., Heiko Anwand, H., Bothmer, V., Davies, J.A., Ergenzinger, K.J.E.,, Halain, J., Hardie, R., Hellin, M., Hinrichs, J., Huke, P., Kennedy, K.V., McQuirk, C., Nicula, B., Renotte, E., Shaugnessy, B.M., Stopfkuchen, L., Tappin, S.J., Tosh, I.A.J., Waltham, N.R., West, M.J.: 2016, A coronagraph for operational space weather prediction. In: *Inter. Conf. Space Optics*, **18**.

Murayama, T.: 1982, Coupling function between solar wind parameters and geomagnetic indices. *Rev. Geophys.* **20**(3), 623. DOI.

Palacios, J., Cid, C., Guerrero, A., Saiz, E., Cerrato, Y.: 2015, Supergranular-scale magnetic flux emergence beneath an unstable filament. *Astron. Astrophys.* **583**, A47. DOI. ADS.

Pesnell, W.D., Thompson, B.J., Chamberlin, P.C.: 2012, The Solar Dynamics Observatory (SDO). *Solar Phys.* **275**, 3. DOI. ADS.

Riley, P., Lionello, R., Mikić, Z., Linker, J.: 2008, Using global simulations to relate the three-part structure of coronal mass ejections to in situ signatures. *Astrophys. J.* **672**, 1221. DOI. ADS.

Sachdeva, N., Subramanian, P., Colaninno, R., Vourlidas, A.: 2015, CME propagation: Where does aerodynamic drag 'take over'? *Astrophys. J.* **809**, 158. DOI. ADS.

Savani, N.P., Vourlidas, A., Szabo, A., Mays, M.L., Richardson, I.G., Thompson, B.J., Pulkkinen, A., Evans, R., Nieves-Chinchilla, T.: 2015, Predicting the magnetic vectors within coronal mass ejections arriving at Earth, 1: Initial architecture. *Space Weather* **13**, 374. DOI. ADS.

Scherrer, P.H., Bogart, R.S., Bush, R.I., Hoeksema, J.T., Kosovichev, A.G., Schou, J., Rosenberg, W., Springer, L., Tarbell, T.D., Title, A., Wolfson, C.J., Zayer, I.: 1995, The solar oscillations investigation – Michelson doppler imager. *Solar Phys.* **162**(1), 129. DOI. ADS.

Schou, J., Scherrer, P.H., Bush, R.I., Wachter, R., Couvidat, S., Rabello-Soares, M.C., Bogart, R.S., Hoeksema, J.T., Liu, Y., Duvall, T.L., Akin, D.J., Allard, B.A., Miles, J.W., Rairden, R., Shine, R.A., Tarbell, T.D., Title, A.M., Wolfson, C.J., Elmore, D.F., Norton, A.A., Tomczyk, S.: 2012, Design and ground calibration of the helioseismic and magnetic imager (HMI) instrument on the solar dynamics observatory (SDO). *Solar Phys.* **275**(1), 229. DOI. ADS.

Sheeley, N.R., Walters, J.H., Wang, Y.-M., Howard, R.A.: 1999, Continuous tracking of coronal outflows: Two kinds of coronal mass ejections. *J. Geophys. Res.* **104**, 24739. DOI. ADS.

Stone, E.C., Frandsen, A.M., Mewaldt, R.A., Christian, E.R., Margolies, D., Ormes, J.F., Snow, F.: 1998, The advanced composition explorer. *Space Sci. Rev.* **86**, 1. DOI. ADS.

Thernisien, A.: 2011, Implementation of the graduated cylindrical shell model for the three-dimensional reconstruction of coronal mass ejections. *Astrophys. J. Suppl.* **194**, 33. DOI. ADS.

Thernisien, A., Vourlidas, A., Howard, R.A.: 2009, Forward modeling of coronal mass ejections using stereo/secchi data. *Solar Phys.* **256**(1), 111. DOI. ADS.

Thernisien, A.F.R., Howard, R.A., Vourlidas, A.: 2006, Modeling of flux rope coronal mass ejections. *Astrophys. J.* **652**, 763. DOI. ADS.

Tousey, R., Howard, R.A., Koomen, M.J.: 1974, The frequency and nature of coronal transient events observed by OSO-7*. In: *Bull. Amer. Astron. Soc.* **6**, 295. ADS.

Tripathi, D., Bothmer, V., Cremades, H.: 2004, The basic characteristics of EUV post-eruptive arcades and their role as tracers of coronal mass ejection source regions. *Astron. Astrophys.* **422**, 337. DOI. ADS.

Volpes, L., Bothmer, V.: 2015, An application of the stereoscopic self-similar-expansion model to the determination of CME-driven shock parameters. *Solar Phys.* **290**(10), 3005. DOI. ADS.

Vourlidas, A.: 2014, The flux rope nature of coronal mass ejections. *Plasma Phys. Control. Fusion* **56**(6), 064001. DOI. ADS.

Vourlidas, A., Ontiveros, V.: 2009, A review of coronagraphic observations of shocks driven by coronal mass ejections. In: Ao, X., Burrows, G.Z.R. (eds.) *AIP Conf. Ser.* **1183**, 139. DOI. ADS.

Vourlidas, A., Lynch, B.J., Howard, R.A., Li, Y.: 2013, How many CMEs have flux ropes? Deciphering the signatures of shocks, flux ropes, and prominences in coronagraph observations of CMEs. *Solar Phys.* **284**, 179. DOI. ADS.

Vršnak, B., Žic, T., Falkenberg, T.V., Möstl, C., Vennerstrom, S., Vrbanec, D.: 2010, The role of aerodynamic drag in propagation of interplanetary coronal mass ejections. *Astron. Astrophys.* **512**, A43. DOI. ADS.

Webb, D.F., Howard, T.A.: 2012, Coronal mass ejections: Observations. *Living Rev. Solar Phys.* **9**, 3. DOI. ADS.

Wood, B.E., Lean, J.L., McDonald, S.E., Wang, Y.-M.: 2016, Comparative ionospheric impacts and solar origins of nine strong geomagnetic storms in 2010-2015. *J. Geophys. Res., Space Phys.* **121**, 4938. DOI. ADS.

Yurchyshyn, V.B., Wang, H., Goode, P.R., Deng, Y.: 2001, Orientation of the magnetic fields in interplanetary flux ropes and solar filaments. *Astrophys. J.* **563**(1), 381. DOI. ADS.